SETEC-MME-79-61
NASA CR-159718
November 1979



# AN INVESTIGATION OF THE INITIATION STAGE OF HOT CORROSION IN NI-BASE ALLOYS

Second Semi-Annual Report

on

Grant No. NSG-3214

Prepared for

National Aeronautics and Space Administration
Lewis Research Center

by

T. T. Huang
G. H. Meier

Department of Metallurgical and Materials Engineering
University of Pittsburgh
Pittsburgh, Pennsylvania 15261

Period Covered: March 1, 1979 - August 31, 1979

## 1.0 Statement of the Problem

The hot corrosion of alloys generally occurs in two stages:

1. An initiation stage which leads to the breakdown of the protective scale,
2. A propogation stage involving rapid reaction between the alloy and the salt or atmosphere.

The critical step in hot corrosion is the destruction of the normally protective oxide layer which separates the fused salt from the substrate. It appears that prevention of hot corrosion must be attained by the prevention of the initiation stage of the reaction. Therefore, an understanding of those processes leading to initiation of hot corrosion should indicate methods of preventing or minimizing alloy degradation.

In the previous report[1] it was concluded that the oxidation rate of $Na_2SO_4$-coated IN-738 between 900 and 1000°C shows an incubation period which is strongly dependent on temperature and salt composition followed by breakaway corrosion originating at sites associated with the presence of carbides in the alloy surface. The present report describes a more detailed study of this phenomenon and the effect of alloy composition, carbide composition and morphology, and alloy heat treatment on the hot corrosion of IN-738 and simpler model alloys.

## 2.0 Experimental

The alloys studied include the commercial Ni-base alloy IN-738 and high purity laboratory alloys prepared to simulate

the effects of the major elements in IN-738. The actual composition of these alloys are:

Ni - 16Cr - 3.4Ti
Ni - 16Cr - 3.4Al
Ni - 16Cr - 3.4Al - 3.4Ti
Ni - 16Cr - 3.4Al - 1.7Mo
Ni - 16Cr - 3.4Al - 2.6W
Ni - 16Cr - 3.4Al - 1.7Ta
#8 Ni - 16Cr - 3.4Al - 1.7Mo - 2.6W
#9 Ni - 16Cr - 3.4Al - 3.4Ti - 1.7Mo
#10 Ni - 16Cr - 3.4Al - 3.4Ti - 2.6W
#11 Ni - 16Cr - 3.4Al - 3.4Ti - 1.7Ta
#12 Ni - 16Cr - 3.4Al - 3.4Ti - 2.6W - 1.7 Mo
#13 Ni - 16Cr - 3.4Al - 3.4Ti - 1.7Mo- 2.6 W - 1.7Ta
AC #13 Ni - 16Cr - 3.4Al - 3.4Ti - 1.7Mo- 2.6 W - 1.7Ta -0.17C
AC #14 Ni - 16Cr - 3.4Al - 3.4Ti - 1.7Mo- 2.6 W - 1.7Ta -8.5Co-1.0Cb-0.17C
and
AC #15 Ni - 16Cr - 3.4Al - 3.4Ti - 1.7Mo- 2.6 W - 8.5Co -1.0 Cb -0.17C

The laboratory alloys were tungsten arc melted under an argon atmosphere, remelted several times, and drop-cast into a water cooled copper chill. The alloys were homogenized for 72 hours in evacuated quartz capsules at 1050°C. The commercial alloy IN-738 was supplied by INCO as 2 3/4 inch diameter bar in the as-vacuum cast condition. Portions of the commercial alloy were remelted and chill cast to refine the carbide size. Specimen coupons were cut from the alloys, polished through 600 grit silicon carbide and cleaned ultrasonically. The salt coatings were supplied by spraying with their aqueous solutions while the coupons were heated using a hot plate and a heat lamp. Coating weights were generally 1 $mg/cm^2$.

A continuous reading Cahn microbalance was used to record weight changes at temperatures between 900 and 1000°C at 1 atmosphere pressure of slowly flowing oxygen. The reaction was initiated by raising a preheated furnace around the quartz furnace tube in which the specimen was supported with oxygen flowing. The furnace

was raised in a time period of ten seconds. At 900°C the system and specimen came to thermal equilibrium in less than one minute. Oxidized specimens were studied using optical and scanning electron metallography and x-ray diffraction. The composition of the salt remaining on the specimens was studied by dissolving the salt in boiling water and analyzing the solutions using atomic absorption spectroscopy.

## 3.0 Experimental Results and Discussion

### 3.1 Commercial IN-738

As reported previously the kinetic curve for the oxidation of $Na_2SO_4$- coated IN-738 can be characterized by three stages.

Stage I is an incubation period where a parabolic curve characterizes the reaction rate,

Stage II is a period of accelerated reaction.

Stage III is a breakaway reaction period during which a linear reaction rate obtains. Typical rate curves for several of the alloys studied are presented in Figure 1. The time of breakaway for alloy A has been shown to be temperature dependent with a minimum at about 970°C and longer times at both higher and lower temperatures.

In order to study the hot corrosion reaction of IN-738, and hopefully describe its temperature dependence, a series of specimens were exposed in 1 atm $O_2$ at high temperatures with 1 mg/cm$^2$ $Na_2SO_4$ coatings, and the reaction was interrupted at different times. One group of specimens was dipped into boiling distilled water to wash away the salt remaining on the surface. The water soluble components were subsequently analyzed by means of atomic absorption analysis. The results are presented in Table I. The results show:

(1) $Na_2SO_4$ remains on the surface of the alloy at least 9 hours at this temperature

(2) Significant amounts of chromium were detected in the leaching water, which indicates the following reaction occurs.

$$\frac{3}{2} O_2 + Cr_2O_3 + 2O^{=} = 2CrO_4^{=} \qquad (1)$$

(3) No significant amount of nickel, aluminum or molybdenum was detected.

The water-washed specimens were examined by X-ray diffraction and subsequently sectioned for metallography. Another group of specimens was also sectioned and carefully polished with kerosene to preserve the salt for metallographic examination. The results of optical and scanning electron metallography are as follows:

Stage I:

Figure 2 shows the scale on a specimen, coated with $Na_2SO_4$ (1 mg/cm$^2$) and oxidized at 950°C for 1 hour. It is clear that the scale was broken down locally allowing the molten salt to penetrate to the scale/metal interface. Figure 2 (b) and (c) are higher magnifications of portions A and B. Figure 2 (d) shows a region where the salt has penetrated through the scale in a local region. Sulfides are observed in the scale and at the scale/metal interface. Edax examination has shown that the break in the scale in Figure 2 c has occurred at the site where an alloy carbide was incorporated into the scale.[1]

Figure 3 shows the salt in the scale. The EDAX results indicate $Al_2O_3$ and $Cr_2O_3$ dissolved into the salt and sulfides formed at the scale/metal interface. In order to examine the dissolution of carbides in the salt a specimen of IN-738 was coated with $Na_2SO_4$ (1 mg/cm$^2$) and oxidized at 970°C for 5 minutes. The specimen was then dipped into boiling water for 10 minutes to wash away the remaining salt. Figure 4 (a) shows the surface of this specimen.

The carbides have apparently dissolved into the salt. Figure 4 (b) shows more detail of one of the dissolved carbides. Figure 4 (c) shows another region on the same surface. The white whiskers on the surface are $Al_2O_3$. The mechanism of their formation is not clear at this time. EDAX results indicate the surface scale is primarily $Cr_2O_3$, $TiO_2$, $Al_2O_3$ and NiO. A corresponding EDAX result for the dissolved carbide is also presented in Figure 4 (e).

Stage II:

Figure 5 (a) is a specimen oxidized at 970°C for 6 hours with a 1 mg/cm$^2$ $Na_2SO_4$ coating. The salt trapped in the scale is evident. Due to the low oxygen potential under the scale the salt composition is shifted toward higher sulfur potentials. Sulfides then start to form in the alloy. Figure 5 (b), (c) and (d) shows the details of the regions where sulfides form. The presence of the salt in the scale is obvious. One important feature is the sulfides incorporated into the inner part of the scale. EDAX results presented in Figure 5 (e) indicate a high content of Na, S, Mo, Al, Cr, Ni and Ti at the scale-metal interface. It is probable a liquid solution of $Na_2SO_4$ and $Na_2MoO_4$ exists there with $Cr_2O_3$, $Al_2O_3$, NiO and $TiO_2$ dissolved in it at temperature.

Stage III:

Figure 6 (a) shows an IN-738 specimen which has been oxidized at 970° C for 9 hours under the same conditions as the specimen in Figure 5. The weight gain of this specimen is just at the point where stage II is changing to stage III It is quite clear that extensive sulfidation has occurred locally and the internal oxides which originally were lined up along the scale/metal interface have become continuous. It is quite possible the $Al_2O_3$ particles have dissolved into the

salt at this interface. A high sulfur potential is reached in the salt and sulfur diffuses into the alloy sulfidizing the chromium in the alloy. Figure 6 (b) shows more detail of this region. The outer scale is $Cr_2O_3$ and an Al-rich salt is present at the scale-metal interface. Chromium sulfides have formed in the matrix. Figure 6 (c) and (d) show other portions of the specimen. It is obvious, these reactions occur locally indicating the salt penetration is a local reaction. One important difference between the sulfides formed in Stage I (or early stage II) and stage III is that the sulfides formed in Stage I are mainly (Cr,Ti) sulfides, which are smaller and form at a lower sulfur potential. The sulfides formed in stage III are mainly chromium sulfides. No titanium has been found in these sulfides, which are much larger and require a higher sulfur potential for their formation. Figures 7 (a) and (b) show the scale on a $Na_2SO_4$-coated specimen after oxidation at 970°C for 10 hours. The outer scale is much thicker and again strong sulfidation is evident. The sulfide which forms in this stage consists primarily of (Ni,Cr) sulfide. From Figure 7 (b), it is clear, the sulfidation occurs preferentially along the alloy grain boundaries. Figure 8 (a) shows severe attack at the specimen corner after a longer exposure time. Porous green NiO has formed in this area. The specimen will eventually be almost completely consumed as shown in Figure 8 (b). The specimen has split into three pieces on cooling to room temperature with unreacted alloy in the center.

### 3.2 Remelted IN-738

The above results and the results presented in the previous report[1] indicate a significant role of carbides in the initiation of hot corrosion of IN-738. To further confirm this, a portion of the IN-738 ingot

(which has a large carbide size ≈10 μm as received from INCO) was melted in an Argon atmosphere and drop-cast into a water cooled copper chill with dimensions 1" x 3/8" x 6". This process produced an alloy R-738 with much smaller carbides ≈1μm. Specimens cut from the remelted alloy were coated with $Na_2SO_4$ and subjected to hot corrosion at 970°C. The refined carbide size resulted in a factor of five increase in the time to breakaway over that for the commercial ingot (Fig. 1).

A series of remelted IN-738 specimens were subjected to hot corrosion, and interrupted at different times. The specimens were dipped into boiling water to wash away the remaining salt on the surface and the solution was analyzed by atomic absorption spectroscopy. The results of this analysis are presented in Table II. Again, the results show the $Na_2SO_4$ stays on the surface of the specimen as long as 10 hours. Except for Cr, no significant amount of other water soluble species was found.

Figure 9 (a)-(e) shows the surface of the remelted IN-738, which was coated with $Na_2SO_4$ and oxidized at 970°C for various times. It is clear the carbides dissolve into the molten salt immediately. The attack of the surface is visible in some areas. More detail of some of these regions is shown in Figure 10. Figure 10 (a) shows the region, where large $TiO_2$ crystals form on the surface of a layer of $Cr_2O_3$. In the right side of this picture some $Al_2O_3$ whiskers have grown on the surface while on the left side no $Al_2O_3$ is found. The transition from an $Al_2O_3$ whisker-rich region to a whisker-free region is shown in Figure 10 (b) and more detail of these two regions is shown in Figure 10 (c) and (d). One important difference is that in the whisker-rich region large plates of $TiO_2$ grow along with $Al_2O_3$ whiskers on top of a finer-grained $Cr_2O_3$ layer, while in the whisker-free regions the density and the size of these $TiO_2$ crystals is greatly reduced. The mechanism of growth of these $Al_2O_3$ whisker is not clear, but apparently they can be dissolved into the molten salt.

$TiO_2$ will also be dissolved into the $Na_2SO_4$. Figure 11 (a) and (b) show the surface oxide on two areas of a R-738 specimen reacted for 10 minutes at 970°C. The dissolution of $TiO_2$ is evident. Figure 12 (a) and (b) illustrates the surface of R-738 after reaction under the same conditions for 52 hours. Now most of the $Na_2SO_4$ has evaporated from the surface. No $Al_2O_3$ whiskers are found on this surface and a continuous layer of $Cr_2O_3$ has formed. Some large grains of $TiO_2$ lie on the top of this layer. Cross sections of the above specimens are also included in Figure 13 and Figure 14. Figure 13 (a) illustrates the alloy oxidized at 970°C for 10 minutes with a $Na_2SO_4$ coating. It is clear that the salt penetrated through the outer protective scale. More detail of this region is shown in Figure 13 (b) where the attack of the scale by the salt in the initial stage is evident. Figure 13 (c) and (d) illustrate the alloy after reaction for 30 minutes. The protective scale has started to form but some sulfides can be found in the matrix. The alloy is unaffected by the presence of sulfides for a long time. Figure 14 (a) shows that after one hour of reaction a rather protective scale has formed and possibly some salt is isolated at the scale/metal interface. Figure 14 (b) shows more detail at this interface. Figure 14 (c) shows the specimen after 10 hours at temperature. In some local regions the needle-like internal oxide $Al_2O_3$ particles have become continuous and incorporated into the outer scale. Extensive sulfidation occurs in this region. More detail of this region is shown in Figure 14 (d) and the corresponding EDAX results from this region indicate a high content of Mo,Ta, W and S as well as Ti, Cr and Al are present at the scale/metal interface. However the weight change of the specimen is still small indicating the reaction is restricted to a very small area. The overall weight changes of the specimens were not affected by the presence of the sulfides until 50 hours. Figure 15 (a) and (c) show the specimen reacted for 52 hours. The scale has become rather porous at this time and again the incorporation of the internal $Al_2O_3$ particles into the

outer scale is obvious. Extensive sulfidation is also evident. The sulfur probably penetrates into the matrix along the $Al_2O_3$ stringers, which provide an easy diffusion path. Figure 15 (b) and (d) show the details of the scale/metal interface. Figure 15 (b) illustrates a continuous layer of CrS and Figure 15 (d) indicates a mixture of Al,Cr,S, Mo and W at the scale/metal interface which probably occurs due to the presence of $Na_2SO_4$ and dissolution of oxides into it. The protective scale is then rendered ineffectual, and extensive sulfide formation occurs. Figure 16 (a)-(d) shows the scale of a remelted IN-738 specimen reacted at 970°C for 120 hours. The outer porous scale has peeled off. It is quite clear attack by the sulfides along the grain boundaries will eventually lead to catastrophic degradation of the alloy.

The observations of the hot corrosion of commerical IN-738 and remelted IN-738 suggest the following sequence for the initiation of severe attack (see Fig. 17). Figure 17 (a) shows the salt coating on the surface of the alloy. Initially, the solubility of $Cr_2O_3$ in reagent grade $Na_2SO_4$ is quite low but the salt will dissolve carbides which have high Mo,W,Ta, and Ti contents. This increases the acidity of the salt and, consequently, increases the solubility of $Cr_2O_3$ locally resulting in a path for molten salt to penetrate to the scale-metal interface as shown in Fig. 17 (b). This penetration may be due to the carbide providing a physical discontinuity in the scale as well as a site of locally high $Cr_2O_3$ solubility. As the scale grows the salt will remain at the scale-metal interface where a low oxygen pressure will obtain producing high sulfur pressures and rapid sulfidation (Fig. 17c). This corresponds to the transition from Stage I to Stage II. As sulfidation proceeds increasing amounts of Cr are tied up in the sulfides and a protective scale can no longer be maintained. The subsequent oxidation of the sulfides along the alloy grain boundaries and the Cr-depleted matrix leads to a layered,

porous NiO scale and breakaway oxidation (Stage III)

### 3.3 Effect of Carbide Size and Composition

The following alloys were prepared to examine the effect of carbide composition on the initiation of hot corrosion attack of IN-738 type alloys.

AC # 13 alloy: Ni-16Cr-3.4Al-3.4Ti-1.7Mo-2.6W-1.7Ta-0.17C (Cb free)

AC # 14 alloy: Ni-16Cr-3.4Al-3.4Ti-1.7Mo-2.6W-1.7Ta-8.5Co-1.0Cb-0.17C

AC # 15 alloy: Ni-16Cr-3.4Al-3.4Ti-1.7Mo-2.6W-8.5Co-1.0Cb (Ta free)

Their microstructure and corresponding EDAX analysis of the carbides are shown in Figure 18. In AC #13 there is a high concentration of Ta, W and Ti in the carbide. In AC #14 there is a high concentration of Ta,W,Cb,Mo, and Ti in the carbide and in AC #15 there is a high concentration of Ti,Cb,Mo, and W in the carbide. Specimens cut from the as-cast ingots were subjected to hot corrosion with 1 $mg/cm^2$ $Na_2SO_4$ and $Na_2SO_4$+$TiO_2$ coatings. The reaction curves for these alloys are shown in Figure 19 and Figure 20. It is noteworthy that AC #13 does not undergo severe attack in either case. The major component absent from this alloy is columbium. The columbium in the alloys will preferentially segregate to the carbide during solidification. The role of Cb in promoting hot corrosion attack has been discussed by D. M. Johnson, D.P Whittle and J. Stringer [2] who found the $Na_2SO_4$ coatings had caused an acceleration in the oxidation rate of a Co-4Cb alloy similar to that in Co-7.5W and Co-4 Mo alloys. Therefore, they conclude, in addition to tungsten and molybdenum, columbium can promote hot corrosion by an acidic fluxing reaction. $Cb_2O_5$ has a high affinity for oxide ions, forming double oxides at the alloy/oxide interface, a feature characteristic of hot corrosion. Seybolt[3] found that $Cb_2O_5$ reacted quite readily with $Na_2SO_4$, as did $WO_3$ and $MoO_3$. Therefore, it would be reasonable to assume the addition of $Cb_2O_5$ into $Na_2SO_4$ would promote

hot corrosion of alloy AC #13. Surprisingly, the result of this test illustrated in curve A of Figure 21 indicates that the addition of $Cb_2O_5$ into the $Na_2SO_4$ does not accelerate the reaction of alloy AC #13. However, if 10% $MoO_3$ is added to the salt the alloy will be degraded at a rapid rate as illustrated in curve C of Figure 21. Curve B of Figure 21 also includes the kinetics of a series of AC#13 alloy specimens which have been heat-treated in vacuum at 1180°C for 3,16,48 and 100 hours all of which fall on the same curve. The purpose of this treatment was to coarsen the carbides in the alloy to study the effect of carbide size in inducing hot corrosion attack. The results indicate none of these specimens undergo severe attack. This further points to the crucial role of carbide composition in the hot corrosion reaction. Curve D of Figure 22 shows the addition of 10% $MoO_3$ will also promote hot corrosion attack in a carbon-free alloy (#15), while the additions of $TiO_2$ and $Cb_2O_5$ as shown in curve C of Figure 22, do not effect the hot corrosion resistance of the alloy. By careful examination of the carbide composition in the alloy it was found that the addition of Cb into the alloy also increases the Mo content in the carbides. The reason for this increase is not known but it will definitely enhance the penetration of the salt through the protective scale. Figure 23 illustrates a series of alloy AC #14 specimens which have been heat-treated at 1180°C for 3,16,48, and 100 hours to coarsen the carbides. The results indicate the larger the carbides the easier is salt penetration and the shorter the incubation time. Similar results have also been found at AC #15.

Figure 24 (a) shows the scale of a carbon-free alloy #14 which was oxidized at 970°C for 5 days. A protective scale forms and sulfides are found in the matrix. Figure 24 (b) shows the scale on alloy AC #14 which has been oxidized at 970°C for 4 days with a $Na_2SO_4$ coating. The degradation of the outer scale is obvious. Figure 24 (c) shows the scale on alloy AC #14 which has been vacuum annealed at 1180°C for 48 hours,

and subjected to the same conditions for 50 hours. A porous scale has formed and again extensive sulfidation along the grain boundaries is evident. Figure 25 (a) shows the scale on alloy AC #15 which has been coated with $Na_2SO_4$ and oxidized at 970°C for 5 days. This scale has also become ineffectual. Figure 25 (b) shows more detail of the scale/metal interface where a layer of a Mo-rich phase adjacent to the alloy was identified by EDAX suggesting that an acidic fluxing reaction is probably dominant in the propogation stage for this alloy.

### 3.4 Carbon-Free Alloys

The hot corrosion of carbon-free Ni-16Cr-3.4Al-3.4Ti alloys, taken to be the basis for IN-738 type alloys, has been studied and the effect of individual additions of refractory metals has been evaluated. During oxidation in the absence of $Na_2SO_4$, Ni-16Cr-3.4Al-3.4Ti, Ni-16Cr-3.4Al-3.4Ti-1.7Mo, Ni-16Cr-3.4Al-3.4Ti-2.6W, Ni-16Cr-3.4Al-3.4Ti-2.6W, Ni-16Cr-3.4Al-3.4Ti-1.7Ta, Ni-16Cr-3.4Al-3.4Ti-1.7Mo-2.6W and Ni-16Cr-3.4Al-3.4Ti-1.7Mo-2.6W-1.7Ta all form a continuous $Cr_2O_3$ layer, which is overlaid with a thin layer of $TiO_2$. with internal $Al_2O_3$ particles forming at the scale base. In some regions, internal $TiO_2$ and $Al_2O_3$ stringers tend to form deep into the matrix. The scales on these alloys in simple oxidation are illustrated in Figure 26. It is apparent that the addition of refractory elements into the alloy does not change the scale morphology significantly. The oxidation curves for these alloys with and without the presence of $Na_2SO_4$ are included in Figure 27. The presence of $Na_2SO_4$ accelerates the reaction slightly, and the addition of the refractory elements reduces the hot corrosion attack. Comparing the oxidized specimens with and without the presence of $Na_2SO_4$ deposits (Figure 26 and 28), it can be seen the microstructure of these oxidized specimens were identical except that in the presence of $Na_2SO_4$ a few (Cr, Ti) sulfide particles were observed in the alloy. The addition of the

refractory elements decreases the rate of attack by producing a more acid salt which does not react extensively with the $Cr_2O_3$ scale to form $Na_2CrO_4$. Apparently the decrease in $Na_2O$ activity of the salt is sufficient to minimize the basic attack of $Cr_2O_3$ but not to induce acidic attack.

## 4.0 Summary

The results of this study have shown that the initiation of hot corrosion attack of IN-738 and similar alloys is the result of local penetration of the molten salt through the protective oxide scale. This penetration occurs at sites where alloy carbides have been incorporated in the scale. The mechanism of scale breakdown may be that the carbide provides a physical discontinuity in the scale or that it provides a site where the salt may become very acid and dissolve the $Cr_2O_3$ scale. The observation that the effectiveness of the carbides in initiating scale breakdown is influenced strongly by their composition suggests the latter mechanism may be the most important. It should be pointed out that while the carbides are the most important factor in the initiation stage of hot corrosion of the class of alloys studied here other mechanisms will give similar results for different alloys. For example, thermal cycling or erosion can damage a protective scale to allow penetration of a molten salt through it. Also, preliminary results in the present study show that the presence of transient oxidation products such as NiO on Ni-Al alloys may provide sites for local salt penetration. Scale inhomogeneities reflecting compositional inhomogeneities may also provide similar sites. However, regardless of the particular mechanism, it appears that the initiation stage for the majority of alloys and pure metals is the result of localized penetration of the salt through the scale. Once the salt is beneath the scale the establishment of low $po_2$, high $ps_2$, conditions leading to the propogation stage will be inevitable.

## 5.0 Future Work

The initiation of hot corrosion attack in $Al_2O_3$- forming alloys such as Ni-Al, Ni-Cr-Al, and Co-Cr-Al will be investigated during the next six months. The effect of atmosphere composition eg. $p_{SO_3}$ will be examined carefully. The effect of this variable will also be evaluated for the $Cr_2O_3$-forming, IN-738-type alloys.

Observation of scales using transmission electron microscopy will also begin during this period in an attempt to correlate the fine structure of scales with the factors which lead to initiation of hot corrosion attack.

References


1. T. T. Huang and G. H. Meier, "An Investigation of the Initiation Stage of Hot Corrosion in Ni-Base Alloys" Progress Report on NASA Grant No. NSG-3214, March, 1979. NASA CR-159616.

2. D. M. Johnson, D. P. Whittle, and J. Stringer, Corr. Sci., 15, 721 (1975).

3. A. U. Seybolt, "$Na_2SO_4$-Superalloy Corrosion Mechanism Studies," General Electric Technical Information Series, 70-C-18p, June 1970.

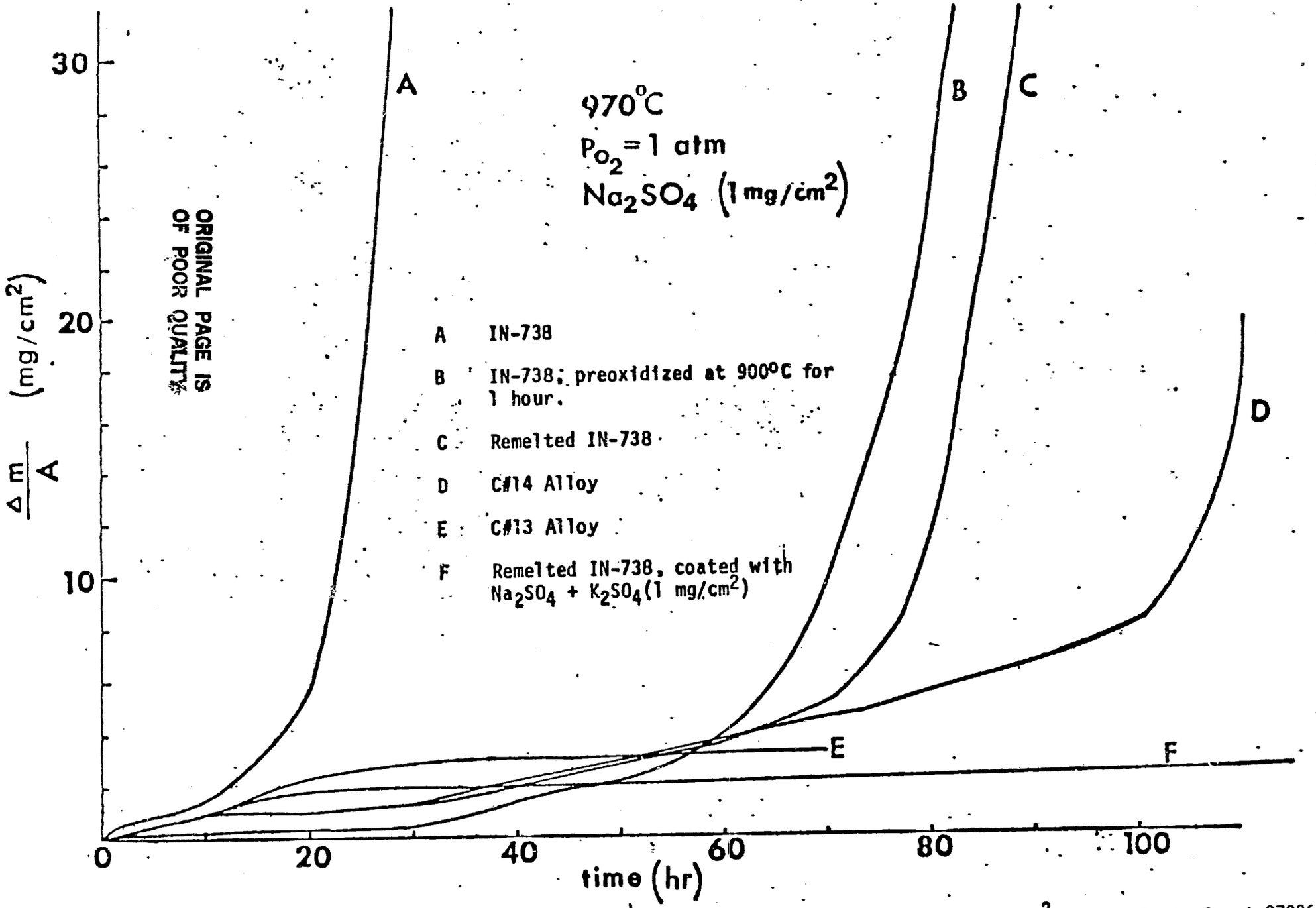


Figure 1 Weight Change vs Time for IN-738 and Several Model Alloys with 1 mg/cm$^2$ Salt in 1 atm $O_2$ at 970°C

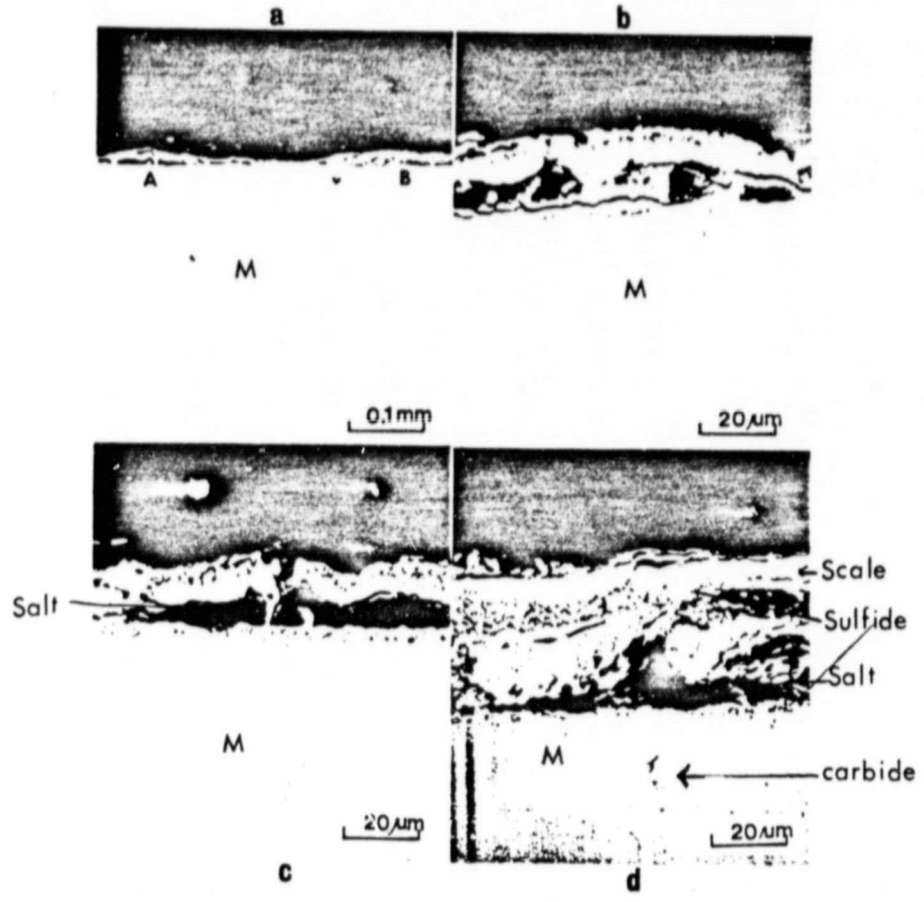


Fig. 2. IN-738 coated with 1 mg/cm$^2$ $Na_2SO_4$ Oxidized at 950°C for 1 hour

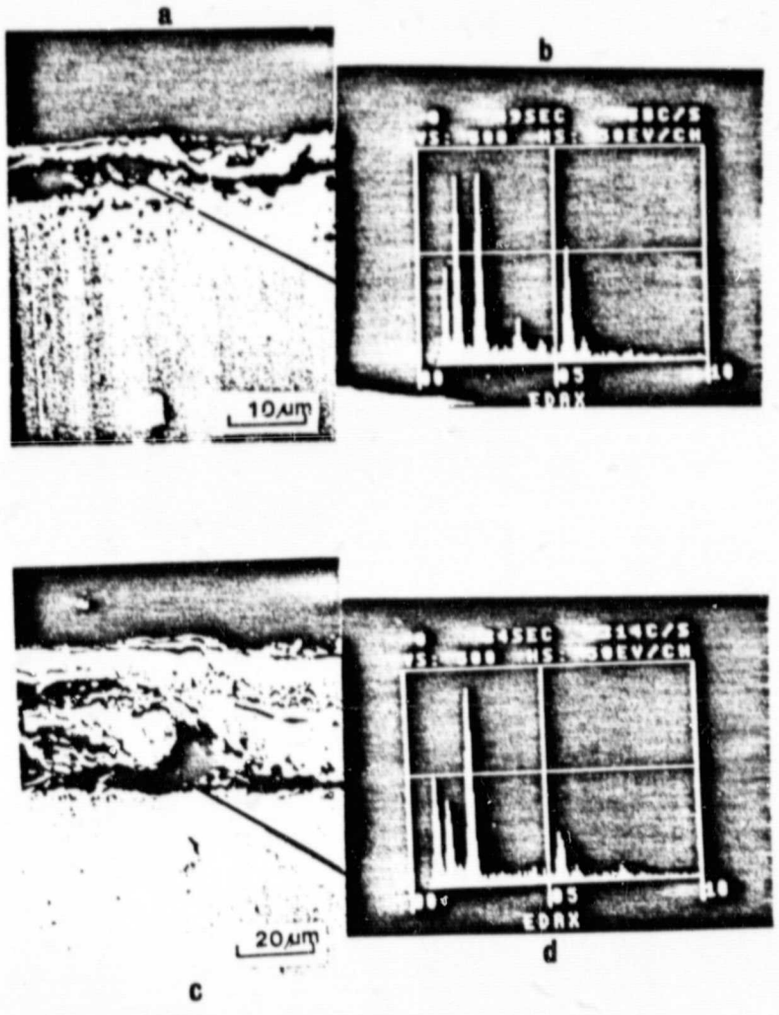


Figure 3. IN-738 coated with $NaSO_4$, oxidized at 950°C for 1 hour


oxide

carbide

Figure 4. IN-738 oxidized at 970°C for 5 min. with 1 mg/cm$^2$ $Na_2SO_4$ , then dipped into boiling water to dissolve the remaining salt

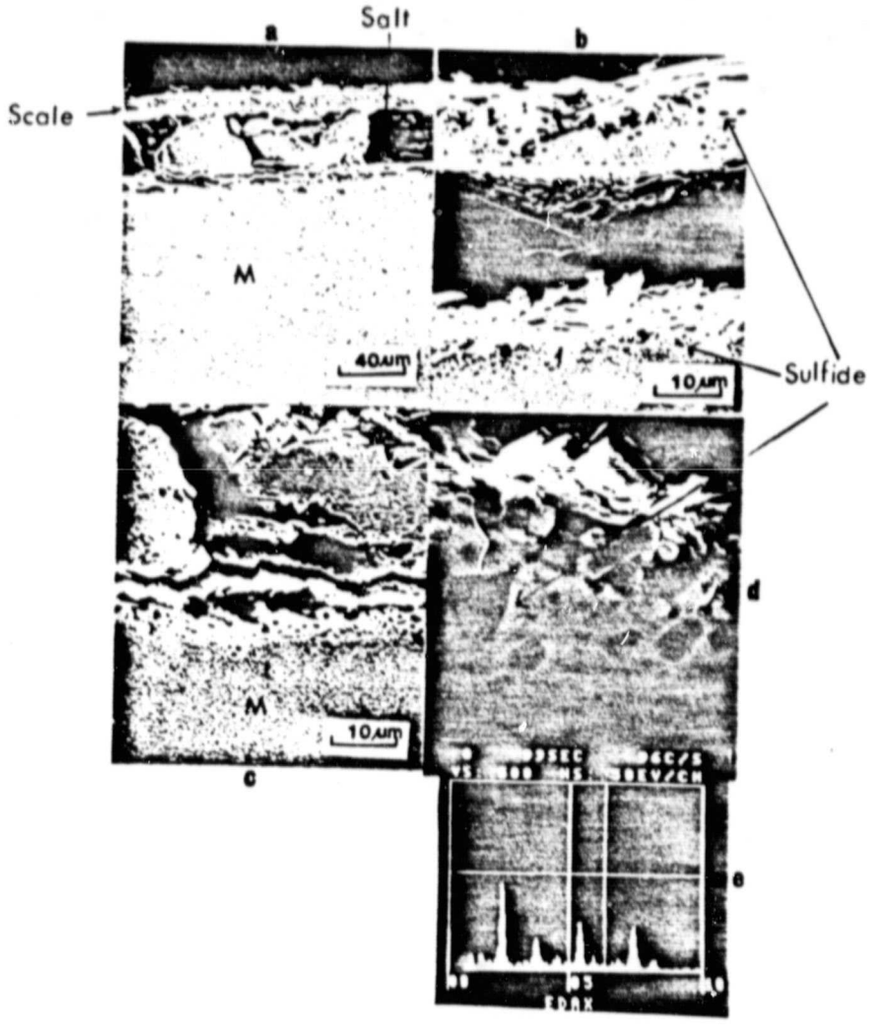


Figure 5.
(a) IN-738 coated with 1 mg/cm$^2$ $Na_2SO_4$, oxidized at 970°C for 6 hours
(b) (c) (d) detail of (a)
(e) EDAX of the scale/metal interface

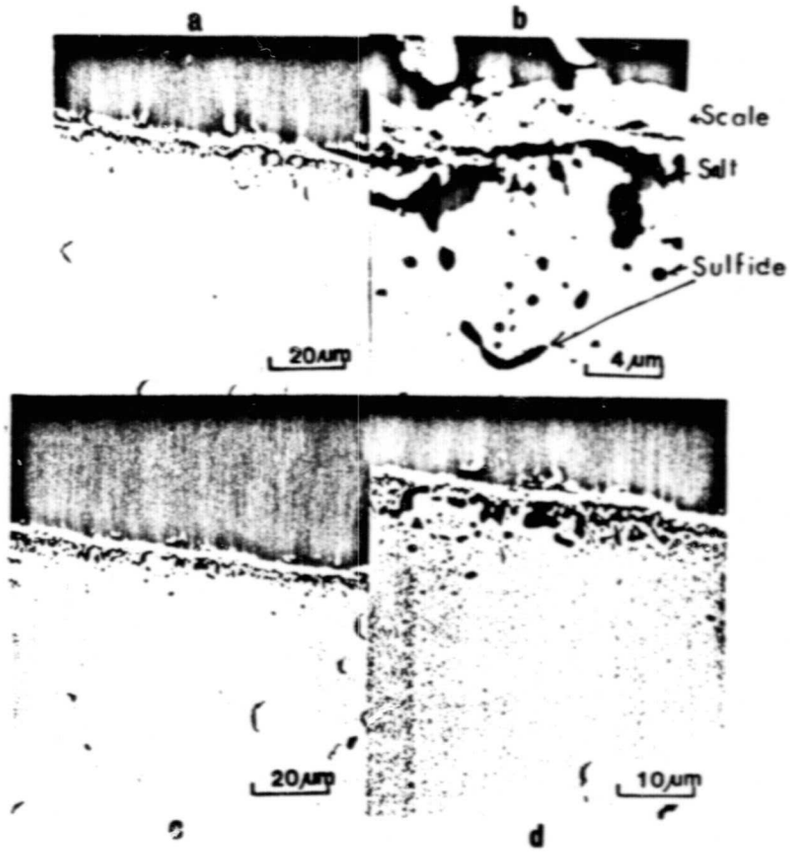


Figure 6. (a) (c). IN-738 coated with 1 mg/cm$^2$ $Na_2SO_4$, oxidized at 970°C for 9 hr. (b). detail of (a). (d) detail of (c).

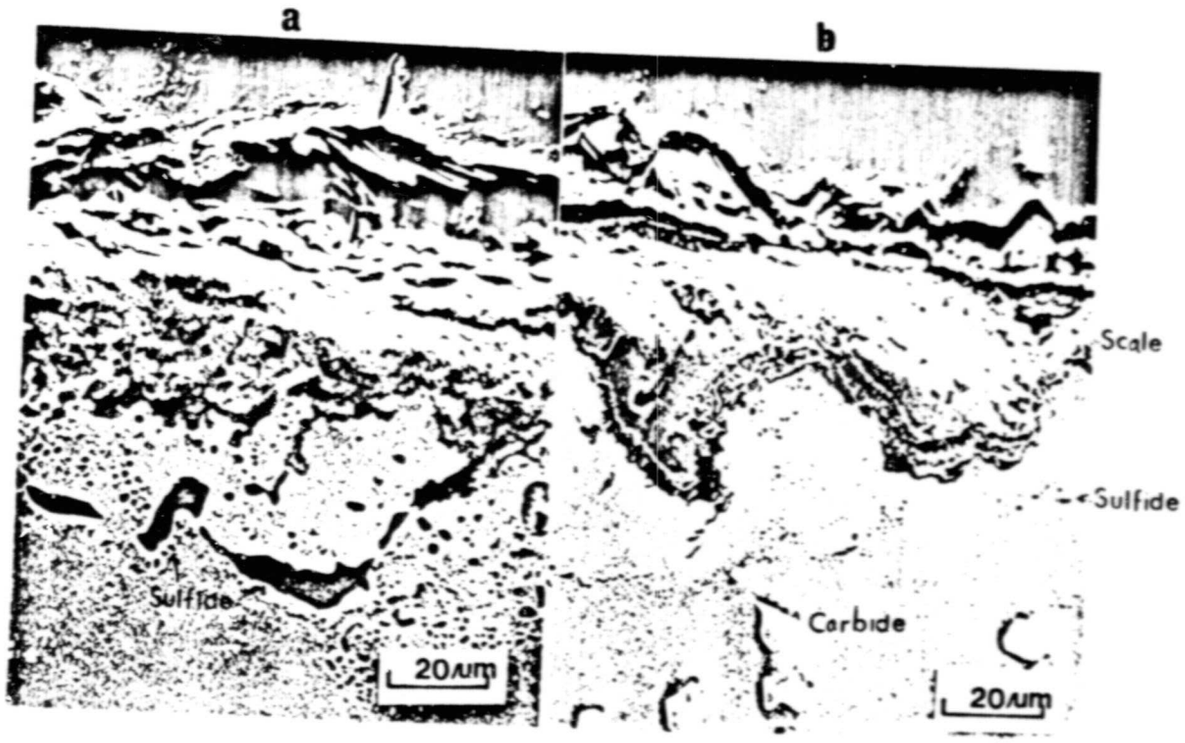


Figure 7. IN-738 coated with 1 mg/cm$^2$ $Na_2SO_4$ and oxidized at 970°C for 10 hours

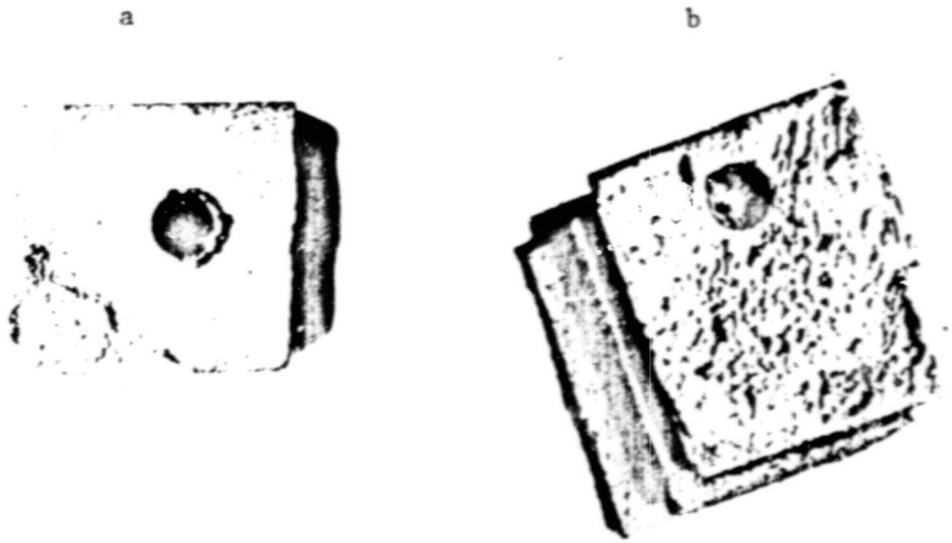


Figure 8. (a) IN-738 coated with $Na_2SO_4$ (1 $mg/cm^2$) , oxidized at 977°C for 8 hours

(b) IN-738 coated with $Na_2SO_4$ (1 $mg/cm^2$) , oxidized at 977°C for 48 hours




Figure 9. Remelted IN-738 coated with 1 mg/cm$^2$ $Na_2SO_4$, oxidized at 970°C for
(a) 10 min. (b) 60 min. (c) 60 min. (d) 30 min. (e) 120 min.

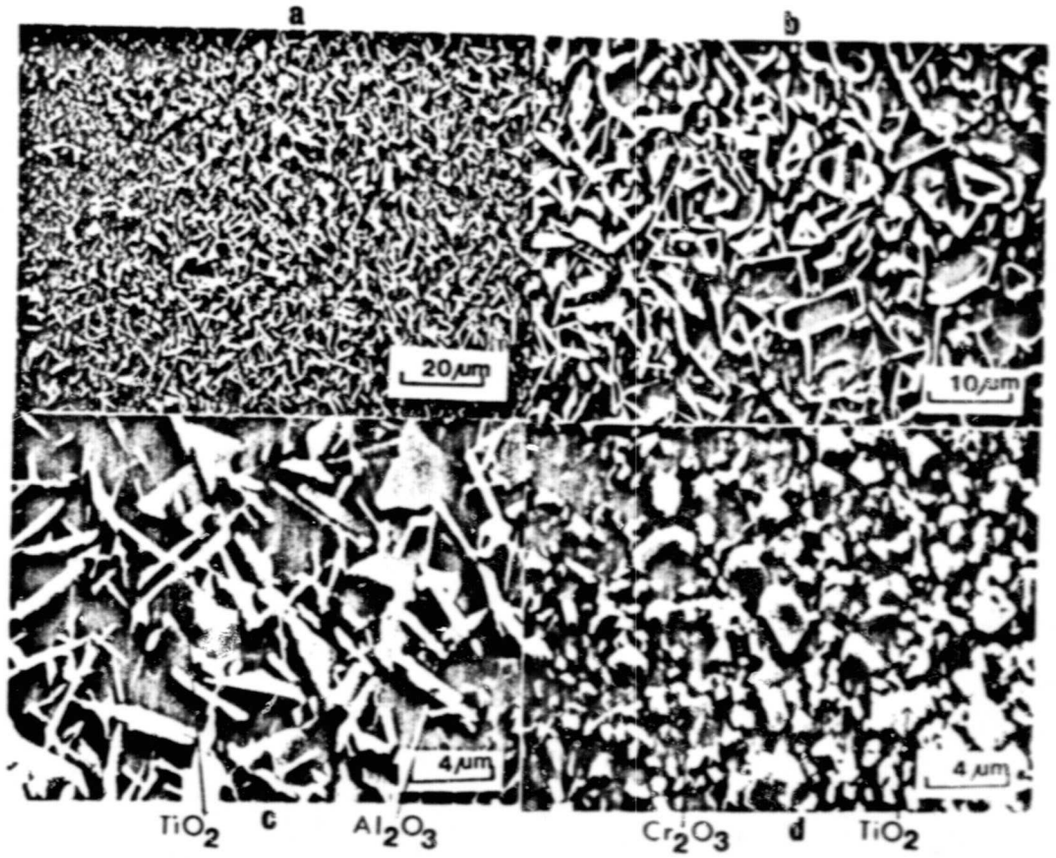


Figure 10. (a) A region on the surface of Remelted In-738 showing the transition from an $Al_2O_3$ whisker-rich region to an $Al_2O_3$ whisker-free region
(b) detail of (a)
(c) $Al_2O_3$ whisker-rich region
(d) $Al_2O_3$ whisker-free region




Figure 11. (a) Remelted IN-738 reacted for 10 minutes at 970°C with 1 mg/cm$^2$ $Na_2SO_4$ coating
(b) Another region of the same specimen showing the dissolution of $TiO_2$

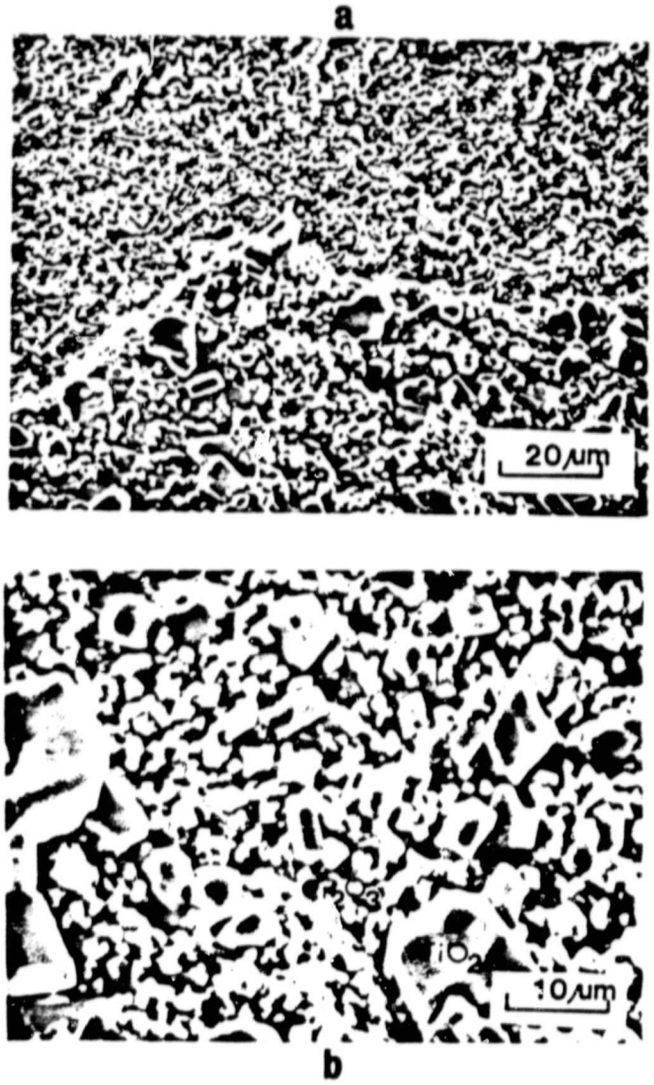


Figure 12. Remelted IN-738 , coated with 1 mg/cm$^2$ $Na_2SO_4$ , oxidized at 970°C for 52 hours

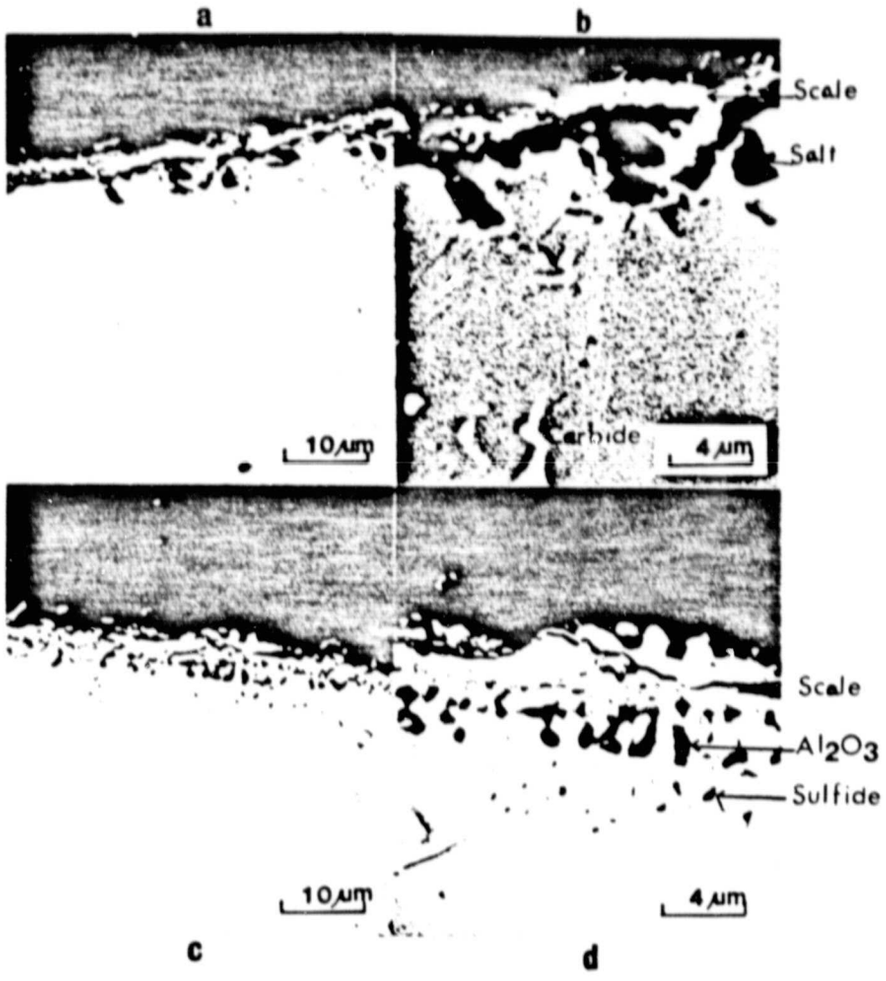


Figure 13. (a) (b) Remelted In-738, coated with $Na_2SO_4$, oxidized at 970°C for 10 min.

(c) (d) Remelted In-738 coated with $Na_2SO_4$, oxidized at 970°C for 30 min.

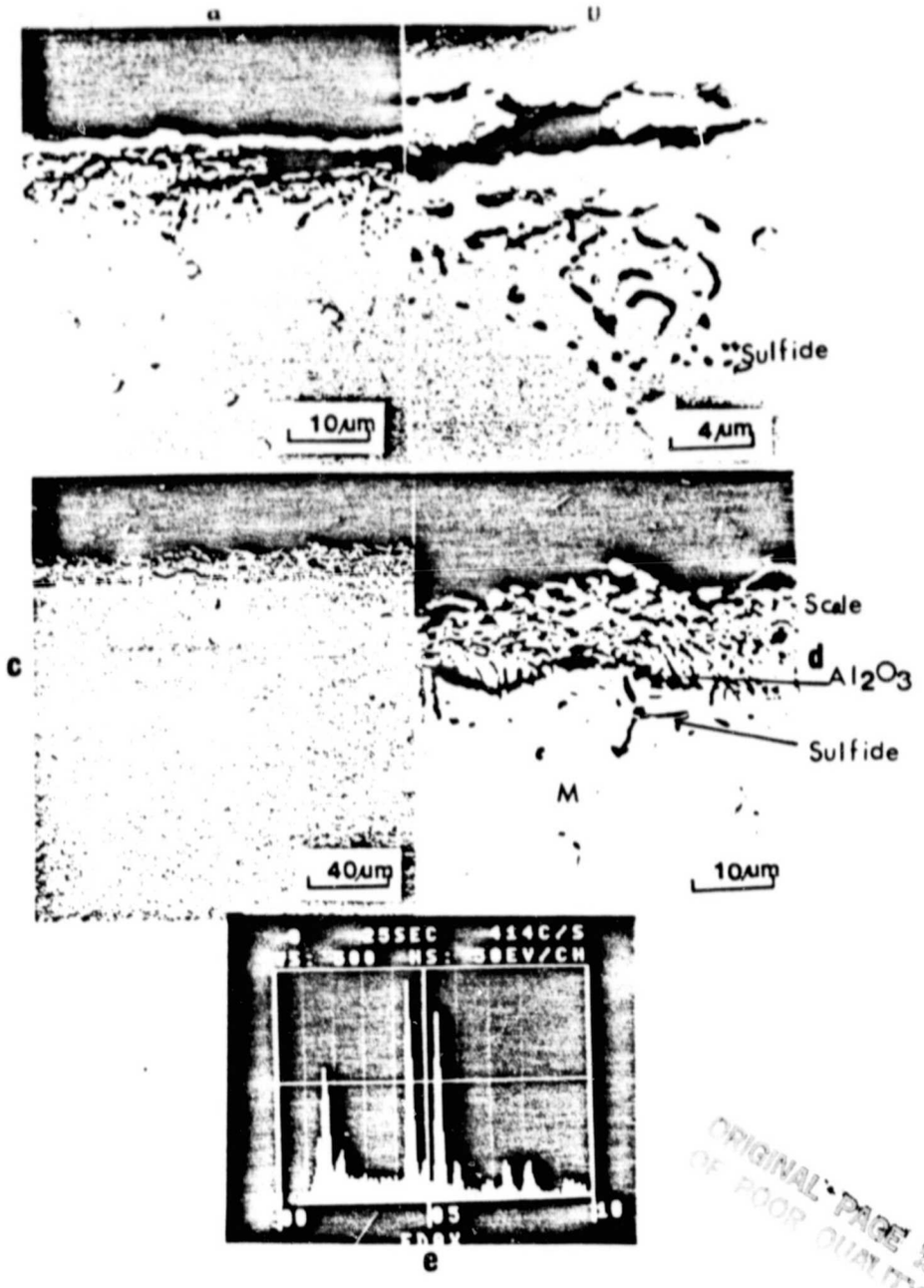




Figure 14. (a) (b) Remelted IN-738 coated with 1 mg/cm$^2$ $Na_2SO_4$, oxidized at 970° for 1 hour
(c) (d) Remelted IN-738 coated with 1 mg/cm$^2$ $Na_2SO_4$, oxidized at 970°C for 10 hours

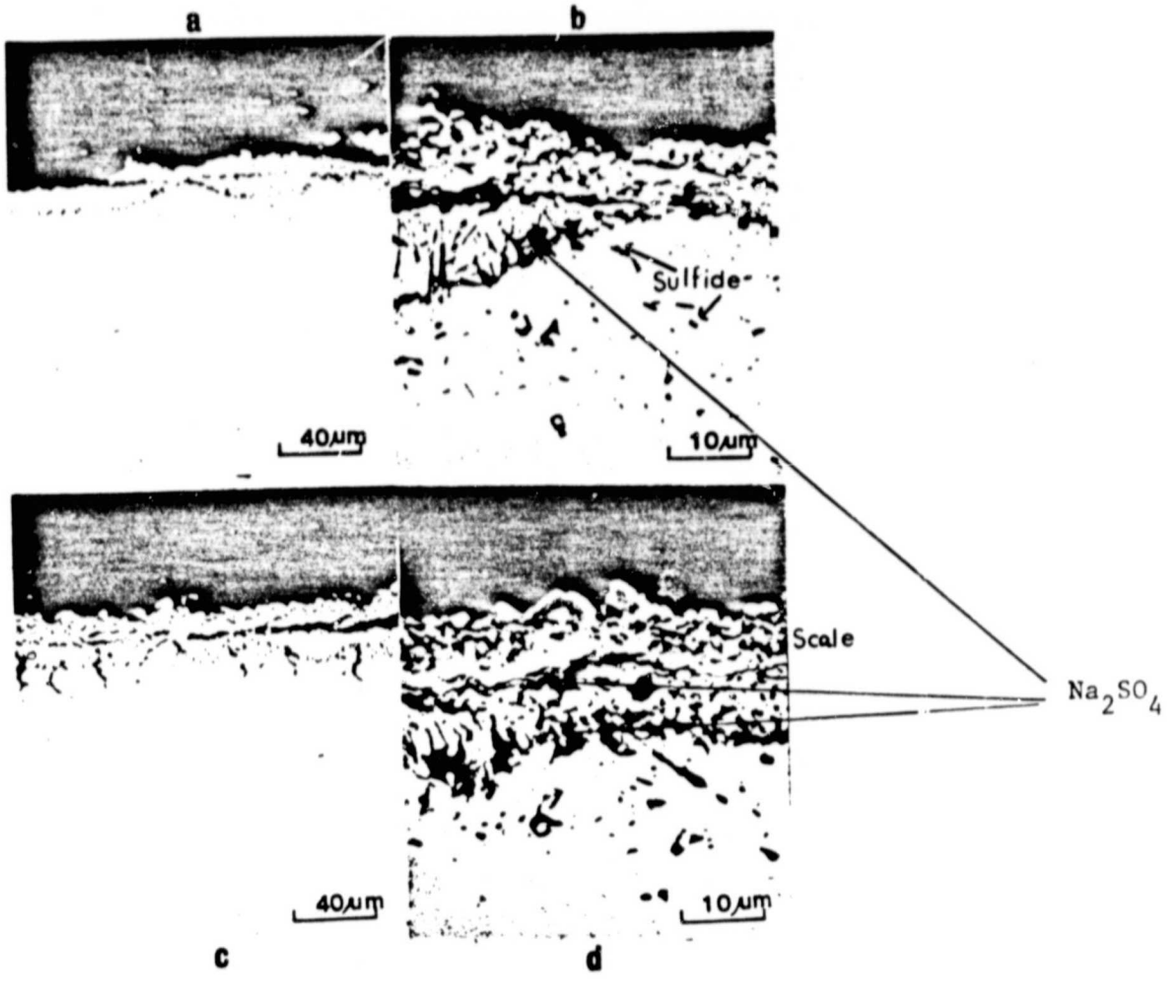


Figure 15. Remelted In-738 coated with $Na_2 SO_4$ , oxidized at 970°C for 52 hours

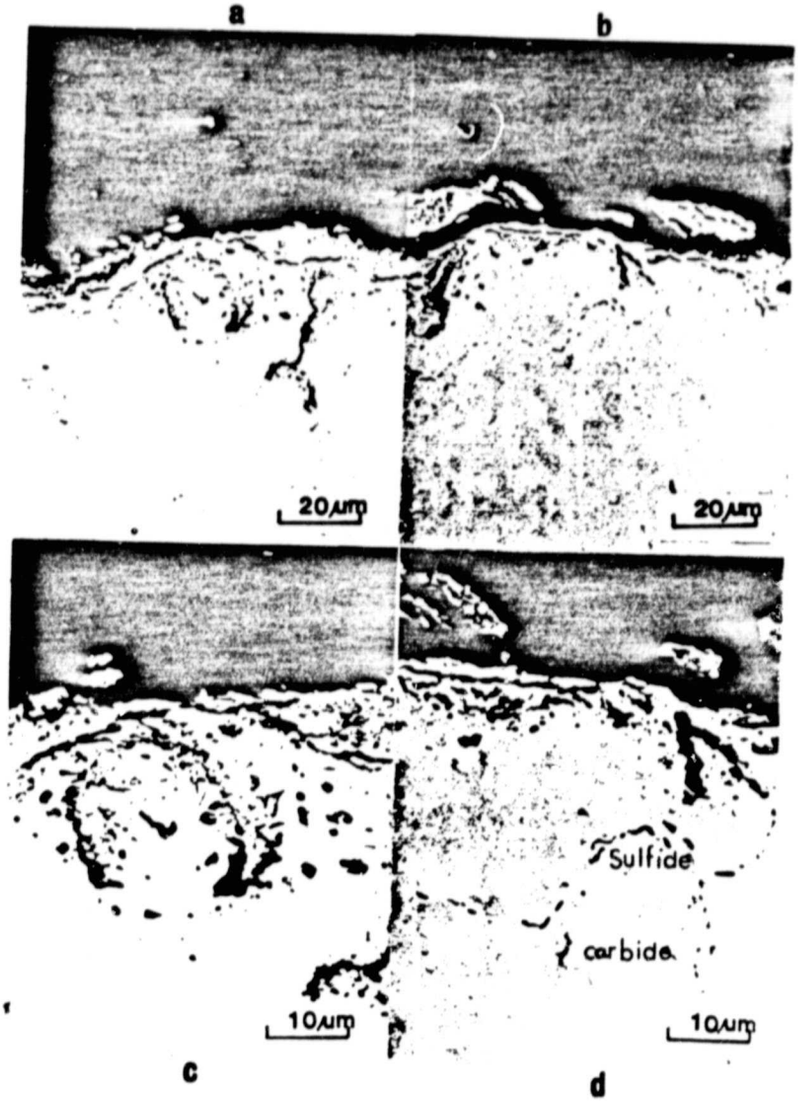




Figure 16. Remelted IN-738 coated with 1 mg/cm$^2$ $Na_2SO_4$ , oxidized at 970°C for 120 hours

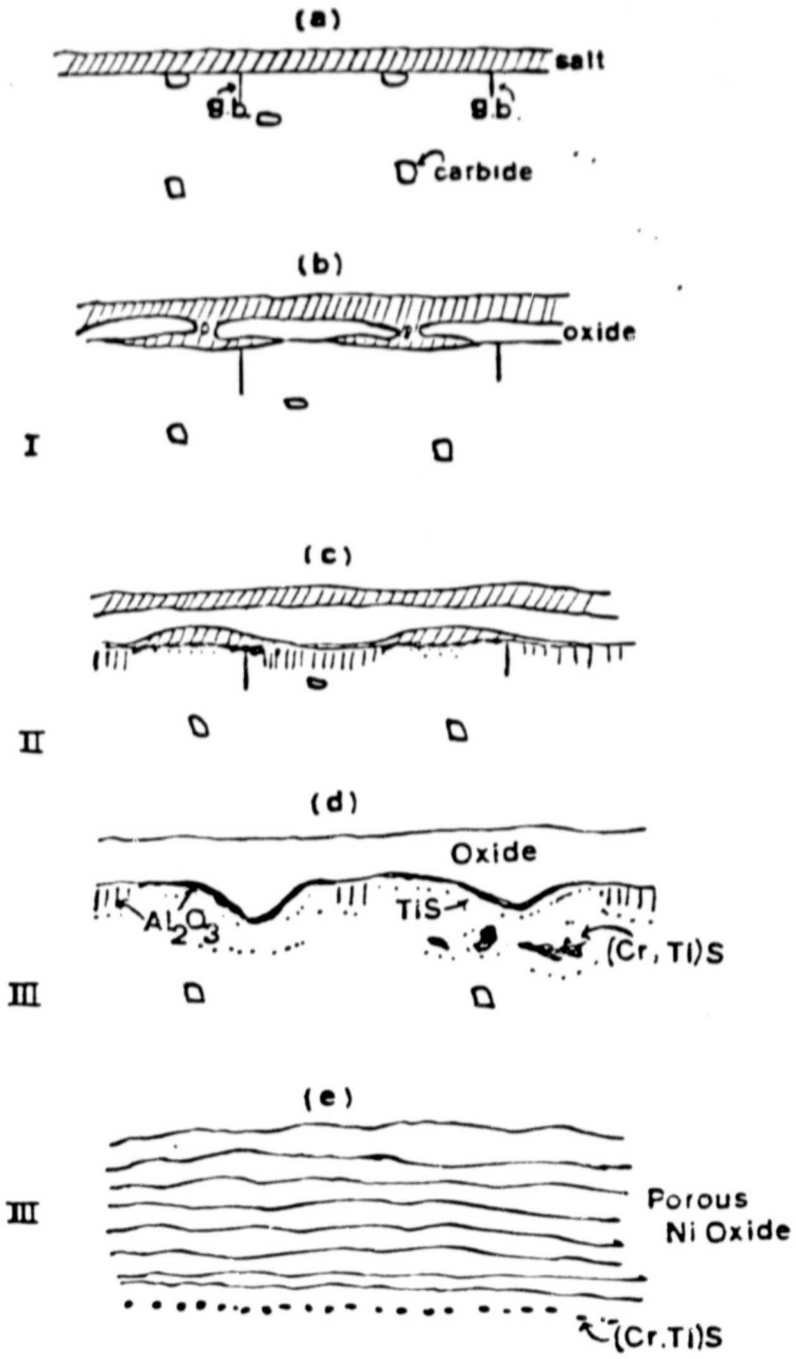


Figure 17. Proposed model for the hot corrosion attack of In-738-type alloys

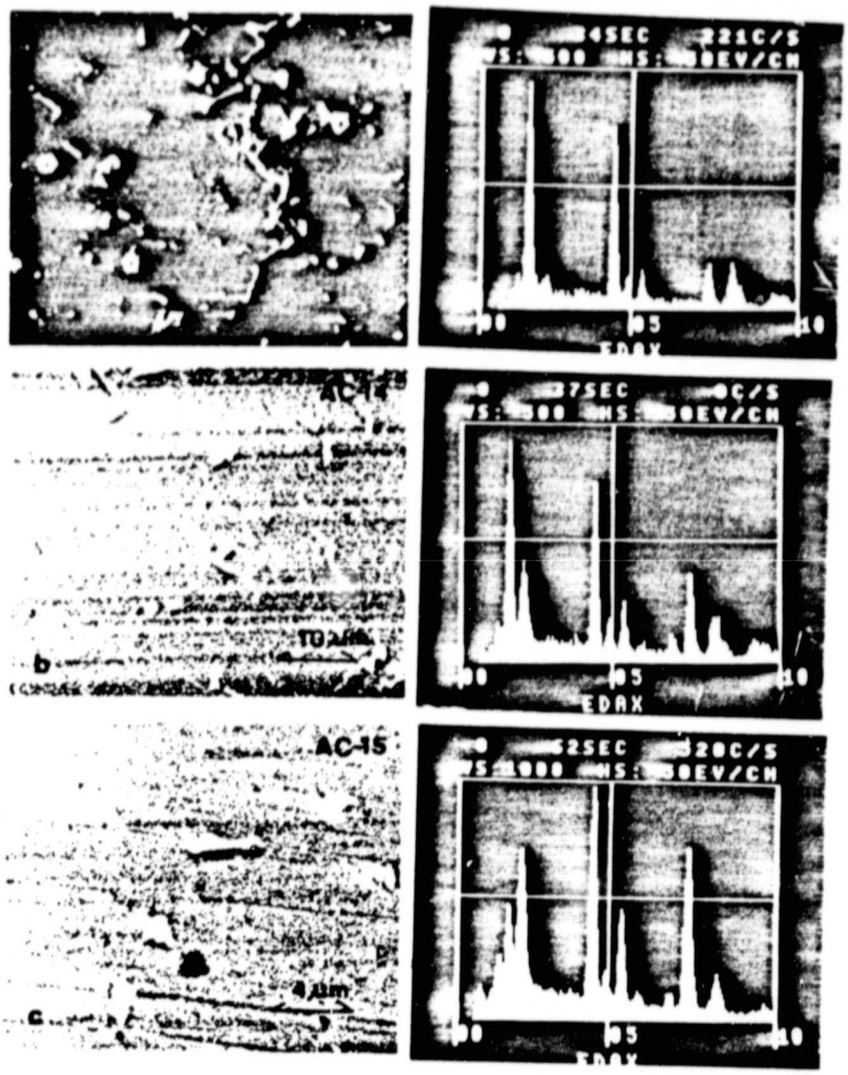


Figure 18. Microstructure and corresponding EDAX Results of the carbides in the alloys:

(a) AC - 13
(b) AC - 14
(c) AC - 15

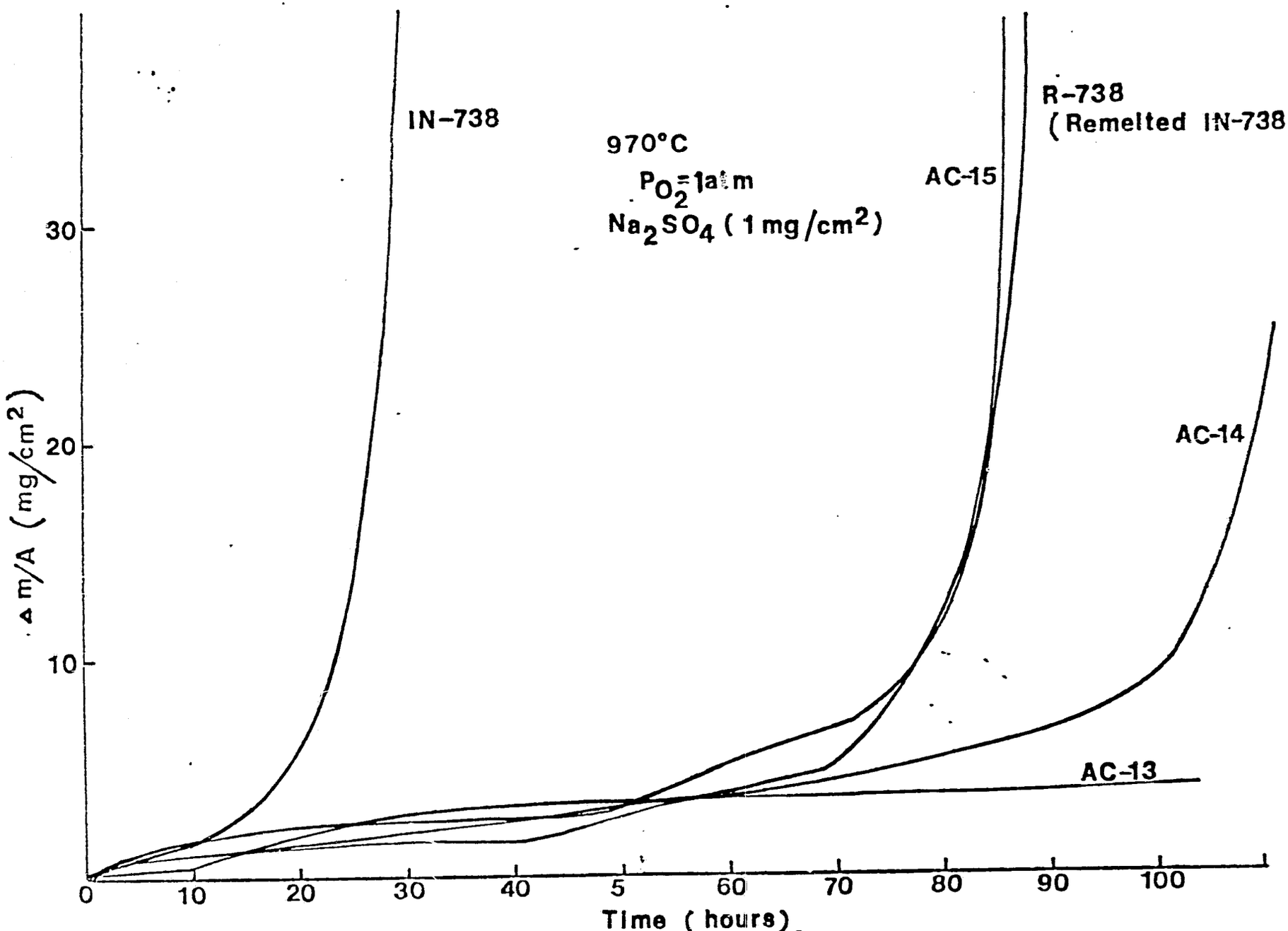


Figure 19. Weight change vs. Time at 970°C with $Na_2SO_4$ (1 mg/cm$^2$) coating for IN-738 like alloys

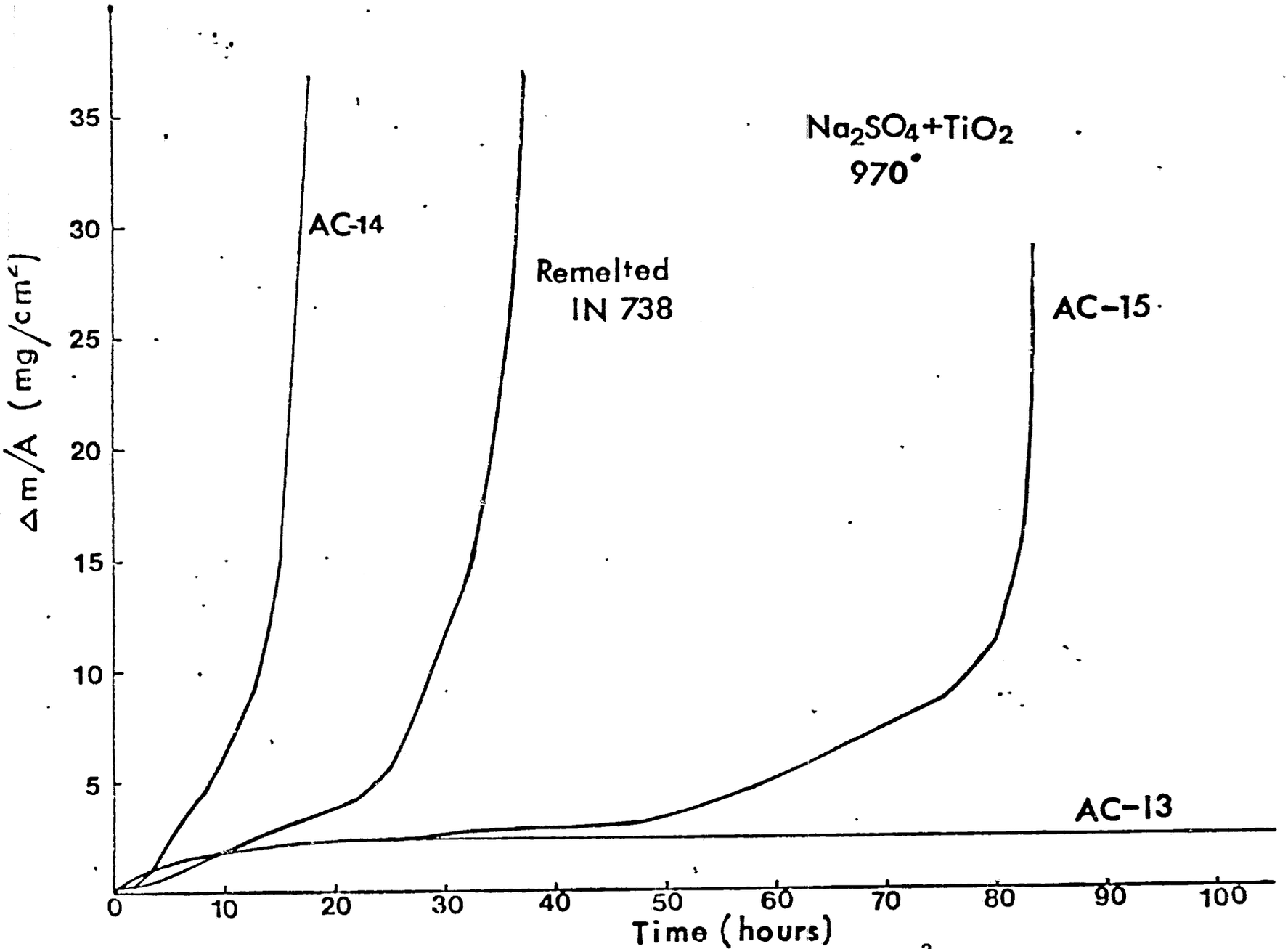


Figure 20. Wt. changes vs. Time at 970°C with $Na_2SO_4$ & $TiO_2$ (1 mg/cm$^2$) coating for IN-738-like alloys

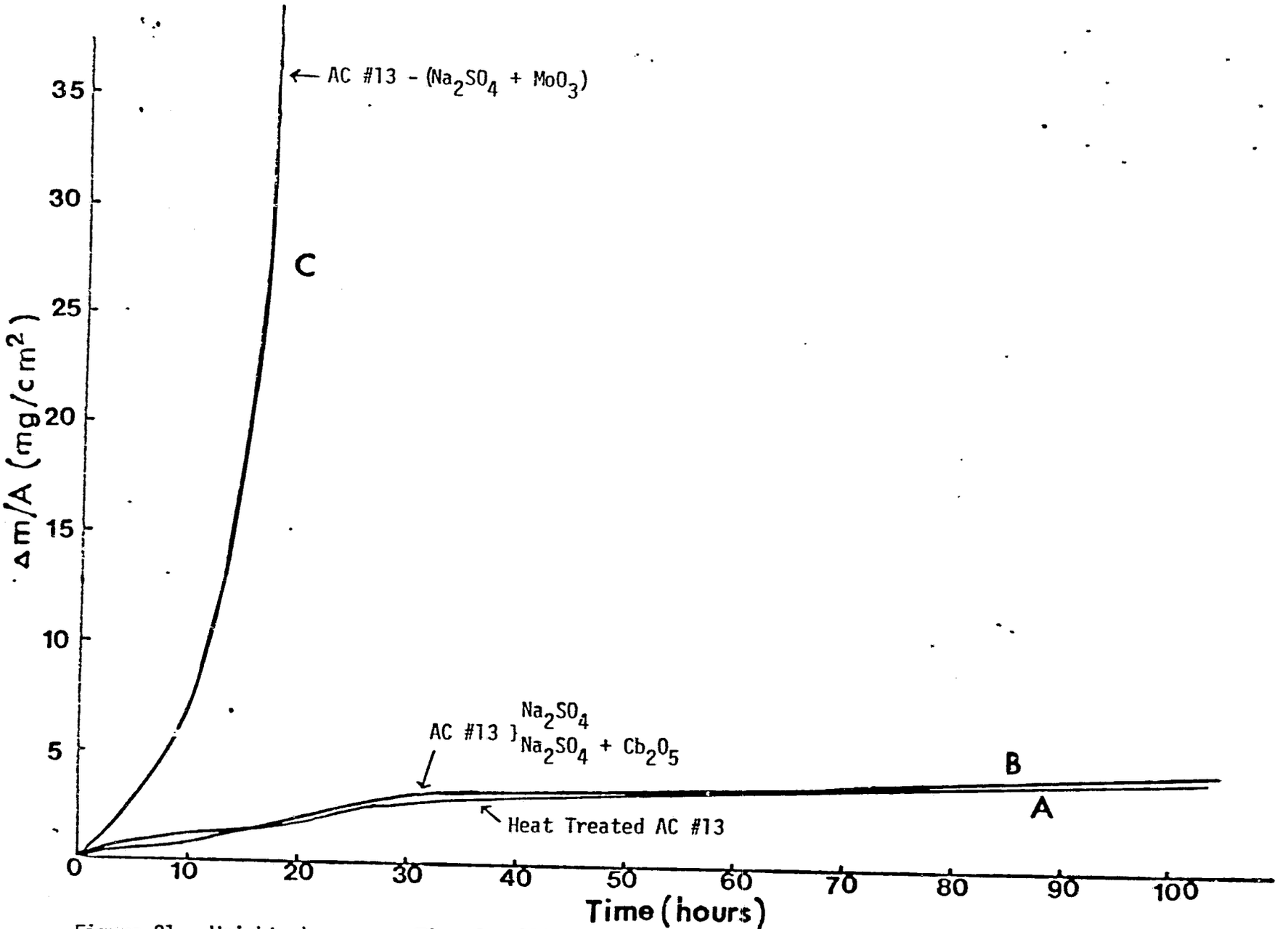


Figure 21. Weight change vs. Time for Alloy AC #13 at 970°C with various salt coatings

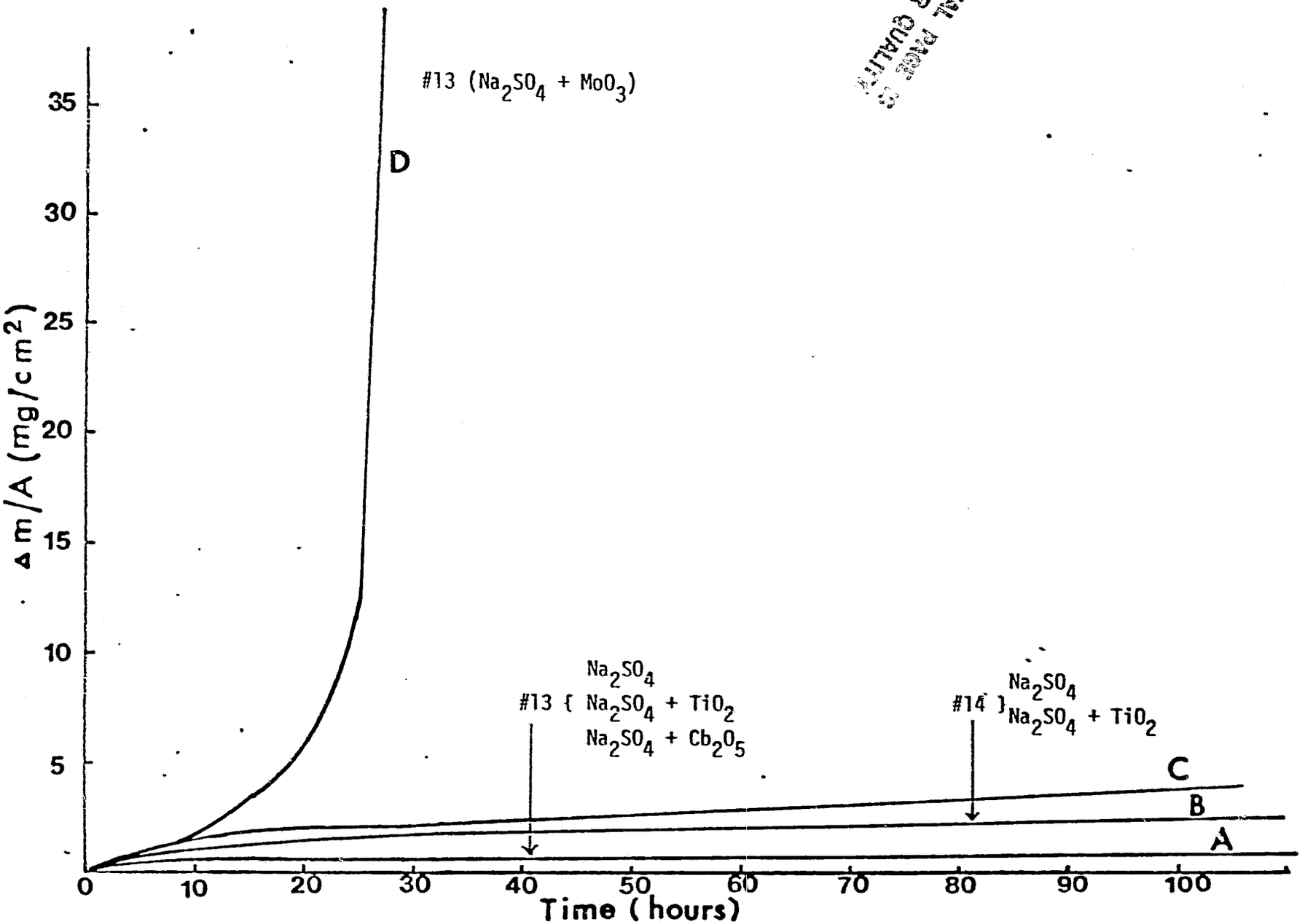


Figure 22. Wt. change vs. Time for carbon free #13 & #14 alloys, oxidized at 970°C with various salt coatings

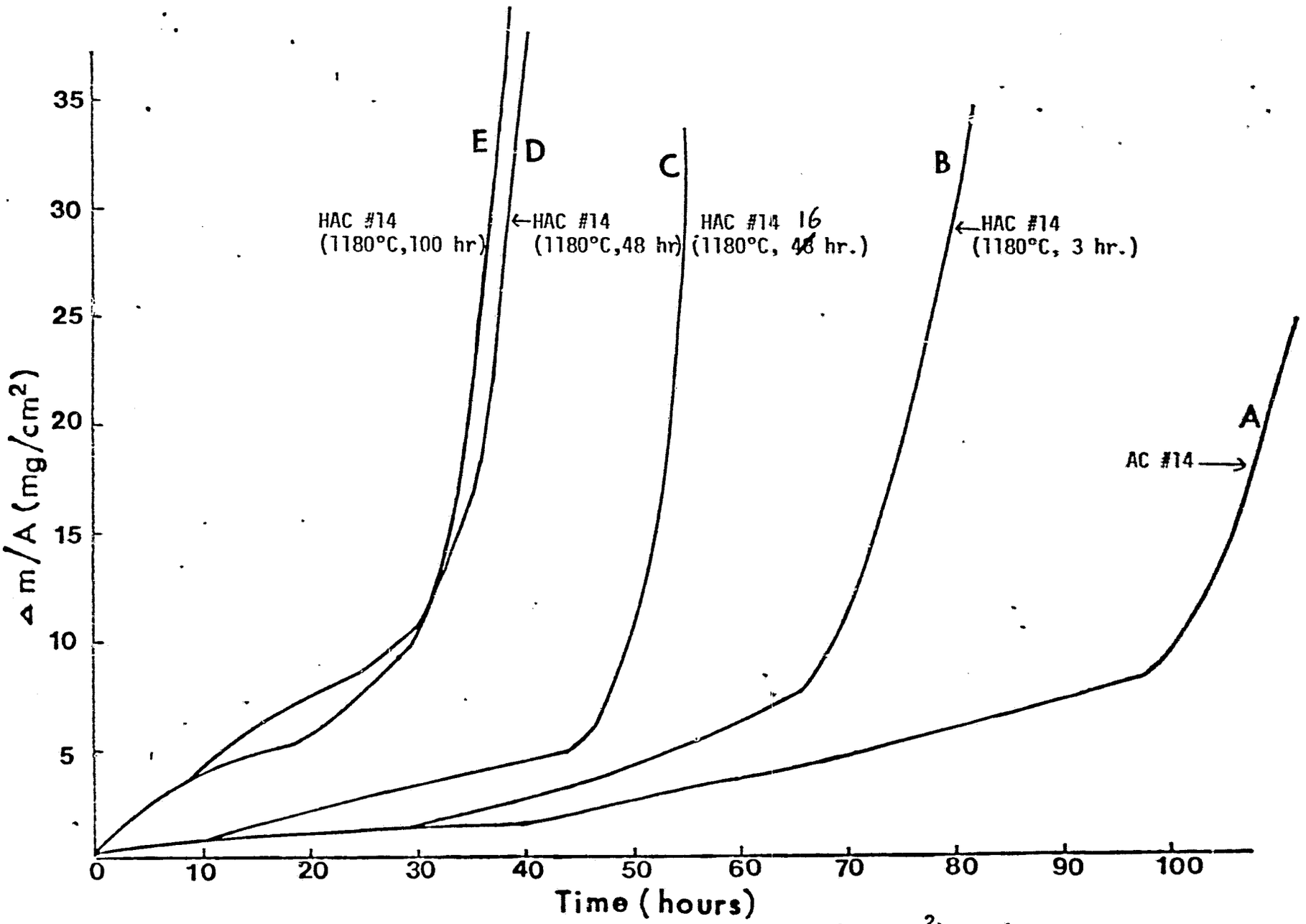


Figure 23. Weight chage vs. Time for AC #14 at 970°C with $Na_2SO_4$ (1 mg/cm$^2$) coating

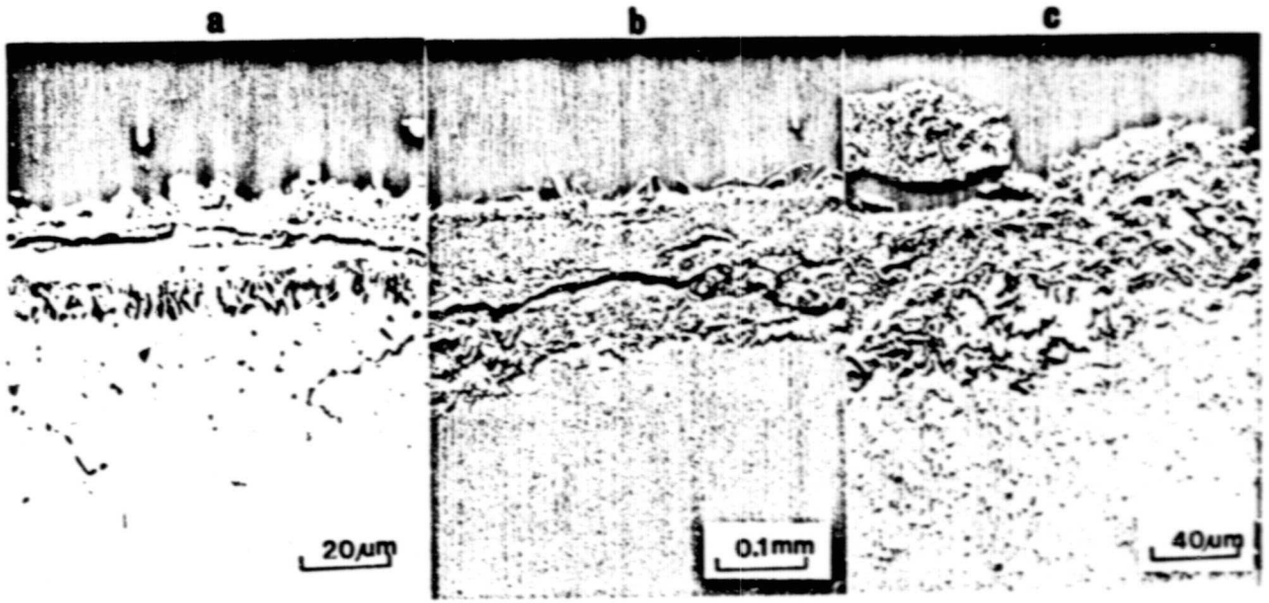


Figure 24. (a) Alloy #14 (carbon free) oxidized at 970°C for 5 days with a 1 mg/cm$^2$ $Na_2SO_4$ coating

(b) Alloy AC #14 oxidized at 970°C for 4 days with a 1 mg/cm$^2$ $Na_2SO_4$ coating

(c) Alloy AC #14 vacuum annealed at 1180°C for 48 hours, and coated with 1 mg/cm$^2$ $Na_2SO_4$ , oxidized at 970°C for 50 hours

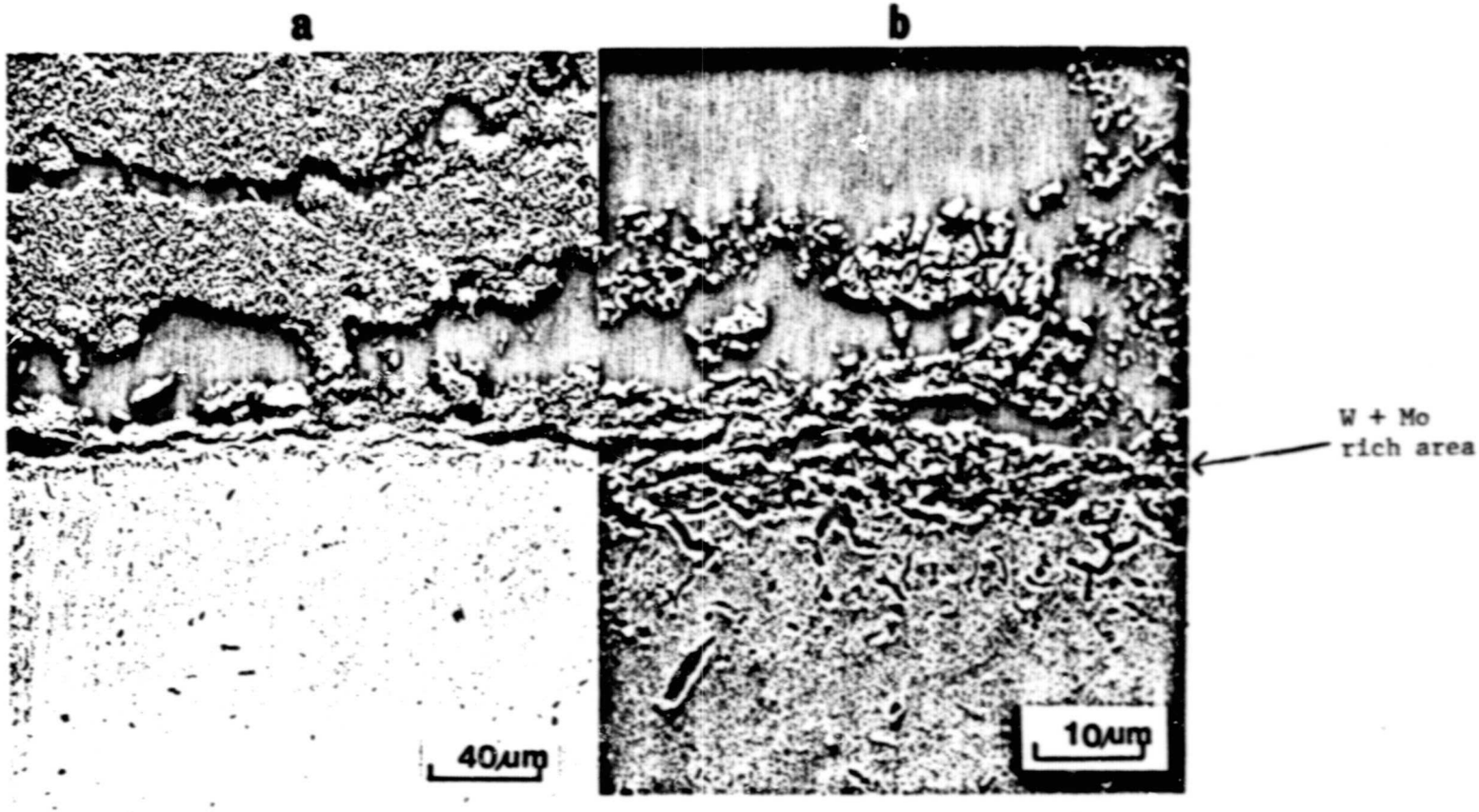


Figure 25. Alloy AC #15 coated with 1 mg/cm$^2$ $Na_2SO_4$, oxidized at 970°C for 5 days

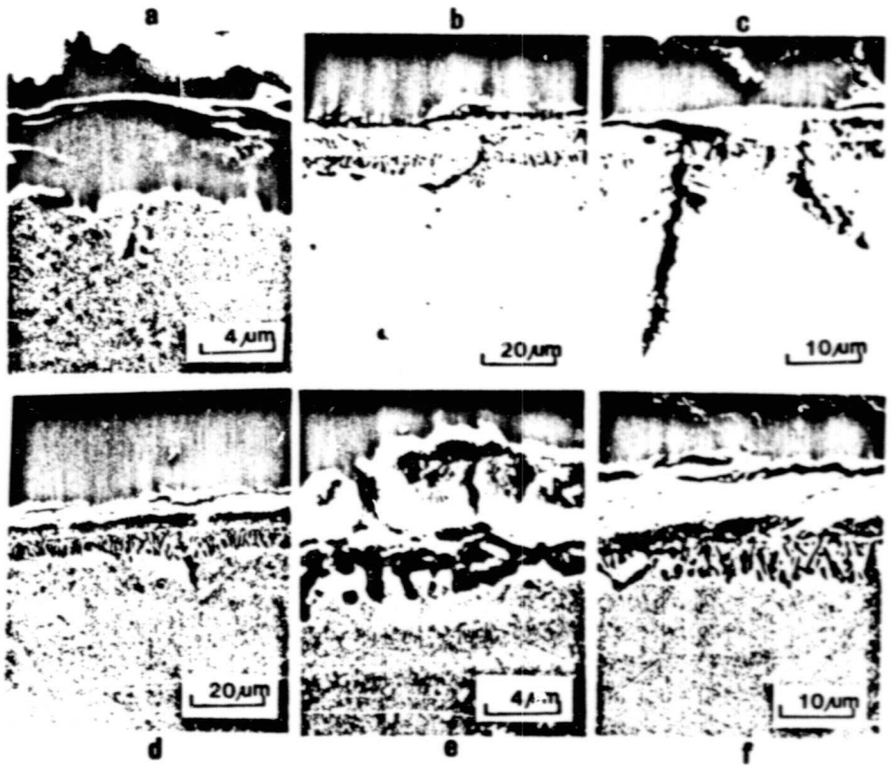


Figure 26. Scales formed in simple oxidation at 970°C on (a) Ni-16Cr-3.4Al-3.4Ti and Ni-16Cr-3.4Al-3.4Ti-x alloys where x is (b) 1.7 Mo, (c) 2.6W, (d) 1.7 Ta, (e) 1.7 Mo+ 2.6W, and (f) 1.7 Mo + 2.6 W + 1.7 Ta

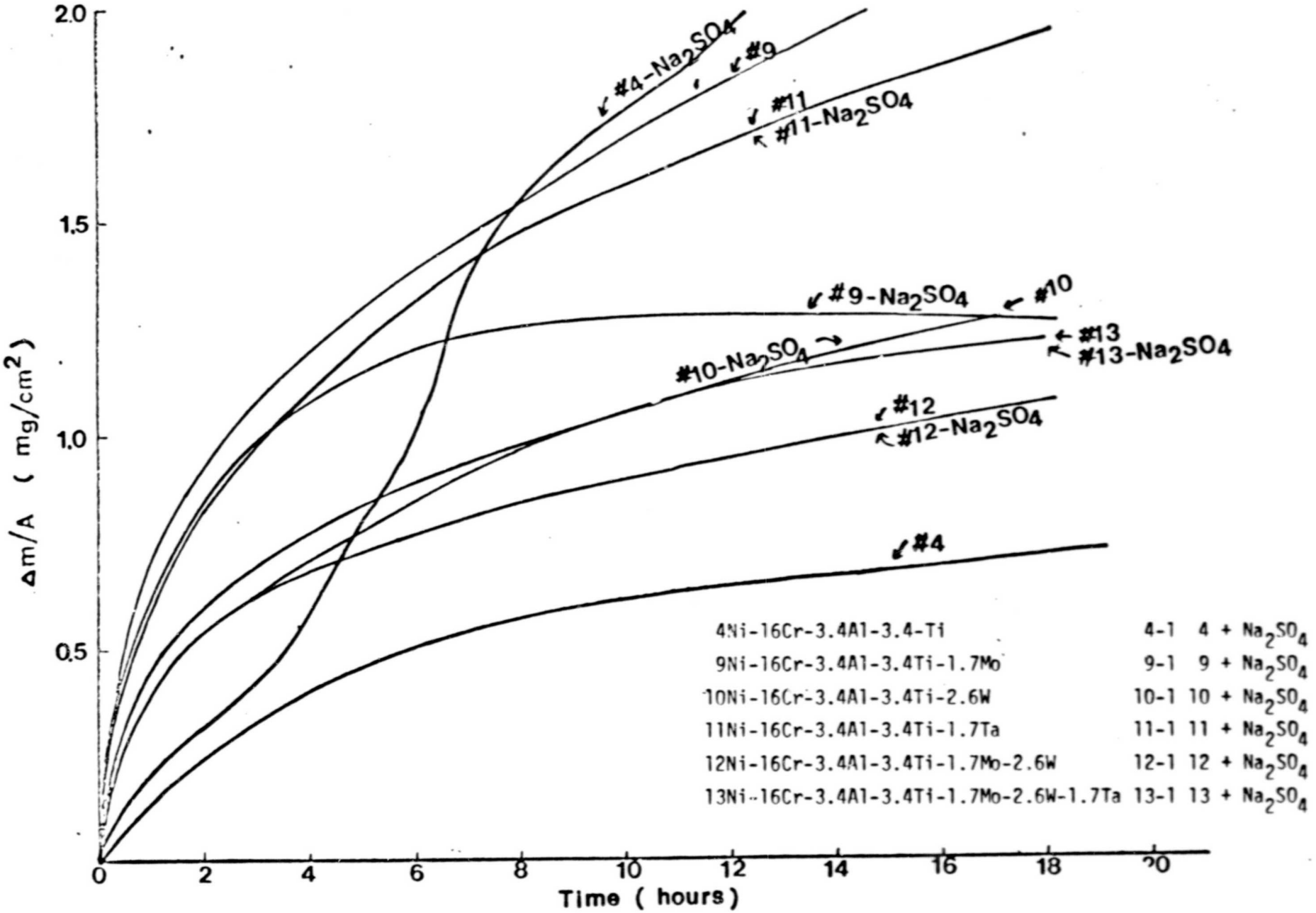


Figure 27. Wt. change vs. Time for various alloys in Simple Oxidation and Coated with $Na_2SO_4$ at 950°C

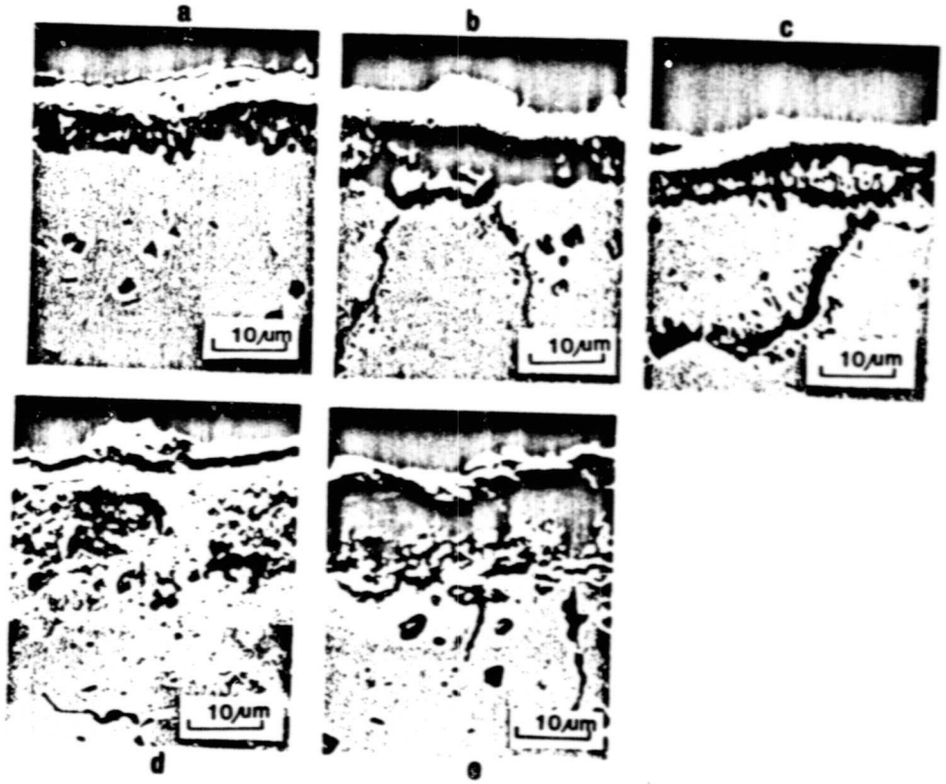


Figure 28. (a) Ni-16Cr-3.4Al-3.4Ti and (b) - (e) Ni-16Cr-3.4Al-3.4Ti-X alloys oxidized at 970°C for 24 hours with a 1 mg/cm$^2$ coating of $Na_2SO_4$. X is (b) 1.7Mo, (c) 2.6W, (d) 1.7Ta, and (e) 1.7Mo + 1.7Ta

Table I: Chemical Analysis of Water Soluble Components in Scales on $Na_2SO_4$ - Coated IN-738 Specimens Exposed in 1 atm $O_2$ at 970°C

| Exposure Time (minutes) | $Na_2SO_4$ on Surface before exposure ($mg/cm^2$) | | | Analysis of water soluble component ($mg/cm^2$) | | | | | | | | |
|---|---|---|---|---|---|---|---|---|---|---|---|---|
| | Total | as $SO_4$ | as $Na^+$ | $Na^+$ | $SO_4^=$ | Cr | Ni ppm | Al ppm | Mo ppm | Ta ppb | Ti ppb | W ppb |
| 10 | 1.01 | 0.684 | 0.326 | 0.307 | 0.544 | 0.008 | <0.1 | <1 | <0.5 | <70 | <0.5 | <30 |
| 30 | 1.02 | 0.688 | 0.332 | 0.288 | 0.453 | 0.041 | | | | | | |
| 60 | 1.201 | 0.813 | 0.388 | 0.290 | 0.473 | 0.076 | | | | | | |
| 120 | 1.178 | 0.798 | 0.380 | 0.396 | 0.529 | 0.112 | | | | | | |
| 260 | 1.025 | 0.694 | 0.331 | 0.316 | 0.43 | 0.140 | | | | | | |
| 540 | 1.09 | 0.738 | 0.352 | 0.356 | 0.43 | 0.188 | | | | | | |

Table II: Chemical Analysis of Water Soluble Components in Scales on $Na_2SO_4$ - Coated Remelted IN-738 Specimens Exposed in 1 atm $O_2$ at 970°C

| Exposure Time (minutes) | $Na_2SO_4$ on Surface before exposure ($mg/cm^2$) | | | Analysis of water soluble component ($mg/cm^2$) | | | | | | | | |
|---|---|---|---|---|---|---|---|---|---|---|---|---|
| | Total | as $SO_4^=$ | as $Na^+$ | $Na^+$ | $SO_4^=$ | Cr | Ni ppm | Al ppm | Mo ppm | Ta ppb | Ti ppb | W ppb |
| 10 | 1.195 | 0.732 | 0.463 | 0.317 | 0.43 | 0.050 | <0.1 | <1 | <0.5 | <70 | <0.5 | <30 |
| 30 | 1.033 | 0.698 | 0.335 | 0.409 | 0.694 | 0.065 | | | | | | |
| 60 | 1.106 | 0.748 | 0.358 | 0.372 | 0.664 | 0.097 | | | | | | |
| 120 | 1.076 | 0.727 | 0.349 | 0.345 | 0.366 | 0.127 | | | | | | |
| 300 | 1.216 | 0.822 | 0.394 | 0.276 | 0.44 | 0.180 | | | | | | |
| 580 | 1.171 | 0.792 | 0.379 | 0.394 | 0.216 | 0.262 | | | | | | |
| 3120 | 1.062 | 0.718 | 0.344 | 0.139 | 0.026 | 0.101 | | | | | | |